Journal of Nuclear Medicine, published on August 28, 2020 as doi:10.2967/jnumed.120.245548

Deep Learning Generation of Synthetic Intermediate Projections Improves ^{177}Lu SPECT Images Reconstructed with Sparsely Acquired Projections

Rydén Tobias.[1], Van Essen M.[2], Marin I.[1], Svensson J.[3], Bernhardt Peter.[1,4*]

[1]Department of Medical Physics and Bioengineering, Sahlgrenska University Hospital, Gothenburg, Sweden

[2]Department of Clinical Physiology, Sahlgrenska University Hospital, Gothenburg, Sweden

[3]Department of Oncology, Institution of Clinical Science, Sahlgrenska Academy, University of Gothenburg, Sweden

[4]Department of Radiation Physics, Institution of Clinical Science, Sahlgrenska Academy, University of Gothenburg, Sweden

First author: Dr. Tobias Rydén

Address: Gula Stråket 2B 413 45 Gothenburg; **Telephone:** +46 748 00 09

E-mail address: tobias.ryden@phonsa.se

***Corresponding author:** Prof. Dr. Peter Bernhardt

Address: Gula Stråket 2B 413 45 Gothenburg; **Telephone:** +46 708 636273

E-mail address: peter.bernhardt@gu.se

Keywords: Dosimetry, ^{177}Lu, Deep-learning, SPECT

Short running title: Synthetic projections improve SPECT

Words: 5000

ABSTRACT

The aims were to decrease ^{177}Lu-SPECT (single-photon emission computed tomography) acquisition time by reducing the number of projections and to circumvent image degradation by adding deep learning–generated synthesized projections.

Method: We constructed a deep convolutional U-structured network for generating synthetic intermediate projections (CUSIP). The number of SPECT investigations was 352 for training, 37 for validation, and 15 for testing. The input was every fourth projection of 120 acquired SPECT projections, i.e., 30 projections. The output was 30 synthetic intermediate projections (SIPs) per CUSIP. SPECT images were reconstructed with 120 or 30 projections, or 120 projections where 90 SIPs were generated from the 30 projections (30-120SIP); using 3 CUSIPs. The reconstructions were performed with two ordered subset expectation maximization (OSEM) algorithms: attenuation-corrected (AC)-OSEM, and attenuation, scatter, and collimator response–corrected (ASCC)-OSEM. Image quality of SIPs and SPECT images were quantitatively evaluated with root mean square error, peak signal-to-noise-ratio (PSNR), and structural similarity (SSIM) index metrics. From a Jaszczak SPECT Phantom, the recovery and signal-to-noise ratio (SNR) were determined. In addition, an experienced observer qualitatively assessed the SPECT image quality of the test set. Kidney activity concentrations, as determined from the different SPECT images, were compared.

Results: The generated SIPs had a mean SSIM value of 0.926 (0.061). For AC-OSEM, the reconstruction with 30-120SIP had higher SSIM (0.993 vs. 0.989; $p<0.001$) and PSNR (49.5 vs. 47.2; $p<0.001$) values than the reconstruction with 30 projections. ASCC-OSEM had higher SSIM and PSNR values than AC-OSEM ($p<0.001$). There was a minor loss in recovery for the 30-120SIP set, but SNR was clearly improved compared to the 30-projection set. The observer assessed 27/30

of the images reconstructed with 30 projections as having unacceptable noise levels, whereas corresponding values were 2/60 for the 30-120SIP and 120 projection sets. Image quality did not differ significantly between the 30-120SIP and 120 projection reconstructions. The kidney activity concentration was similar between the different projection sets, excepting a minor reduction of 2.5% for the ASCC-OSEM 30-120SIP.

Conclusion: Adopting synthetic intermediate projections for sparsely acquired projections considerably recovers image quality and could allow reduced SPECT acquisition time in clinical dosimetry protocols.

INTRODUCTION

Encouraging treatment effects have been reported for ^{177}Lu-pharmaceuticals in somatostatin receptor–positive neuroendocrine tumors and metastatic prostate cancer (*1,2*). ^{177}Lu-DOTATATE was recently approved for treatment of neuroendocrine tumors with a standard protocol allowing a maximum of four treatments with 7.4 GBq. The protocol does not require dosimetry. Nevertheless, a recent prospective dosimetry study demonstrated that an increased number of treatments can be given based on total absorbed kidney dose (*3*), thereby avoiding undertreatment. In addition, dose-response relationships have been reported for the dose-limiting organs kidneys and bone marrow, indicating the potential for dosimetry as one important factor in the individualized treatment protocol (*4,5*).

Recent dosimetry protocols use single-photon emission computed tomography (SPECT) and computed tomography (CT) images or a combination of planar images and SPECT/CT (*4*). In the latter, the kinetics are determined from the planar images and the activity concentration from the SPECT. In a simulation study, the relative uncertainty for kidney absorbed doses was 32% for planar dosimetry and 15% for the planar/SPECT/CT method, which further decreased to 6% for purely SPECT/CT-based dosimetry (*6*). This pattern indicates a clear advantage for SPECT/CT-based dosimetry, but this imaging format is time consuming, and whole-body SPECT/CT with appropriate counting statistics is challenging to obtain.

The SPECT/CT reconstruction methods have gone from a filtered back-projection approach to the iterative ordered subset expectation maximization (OSEM) algorithm (*7*). Today's analytical OSEM reconstruction algorithms, e.g., Evolution, xSPECT, and Flash3D, offer the potential to correct for attenuation, scatter, and collimator-detector resolution, with improved image quality and accuracy in activity quantification (*8*). Further improvements might be achieved by Monte

Carlo (MC)-based OSEM reconstruction methods (*9-11*). According to the EANM/MIRD guideline for quantitative ^{177}Lu SPECT dosimetry, the number of projections should be 60 to 120 (*12*), which was used in recent publications of clinical ^{177}Lu dosimetry (Table 1). An Uppsala group reported the most time-consuming protocols, using 60 or 120 projections with acquisition times of 30 minutes and employing attenuated corrected (AC)-OSEM (*3,13,14*). With this protocol, four data points at 1, 24, 96, and 168 h.p.i. are collected, enabling accurate ^{177}Lu kinetics. However, at many centers, the available camera time is limited, and acquisition times are shorter (*15-22*). A short acquisition time may become problematic when measuring at later time points, due to increased image noise (*17,23*). With the introduction of ^{177}Lu-PSMA for metastatic prostate cancer, SPECT/CT dosimetry requires 2-3 bed positions to cover the critical organs: salivary gland, bone marrow, kidneys, and targets in the pelvis region (*21,24*). Such protocols require restricted acquisition times per bed position for patient comfort and may still need more camera time. In these later studies, attenuation, scatter, and collimator-detector response corrected (ASCC)-OSEM reconstructions are often used for good image quality.

The aim of this study was to reduce the SPECT acquisition time by reducing the number of projections, and compensate the image quality degradation by including synthetic intermediate projections (SIPs) in the reconstruction. We created three convolutional neural networks and trained them to generate 3×30 SIPs from 30 acquired projections. For evaluation, we analyzed the image quality of phantom and patient SPECT images as well as estimating kidney activity concentration for SPECT images reconstructed with the SIPs. Two SPECT/CT reconstruction methods were tested: AC-OSEM and ASCC-OSEM, using MC methodology for the latter.

MATERIALS AND METHODS

Subjects and Image Acquisition

In the study, 304 ^{177}Lu-DOTATATE and 100 ^{111}In-octreotide SPECT image data were retrospectively selected from the examination years 2007–2018. The retrospective use of the image data and waiver of consent were approved by the Regional Ethical Review Board in Gothenburg. The gamma cameras used for the examinations during this period were Millennium VG Hawkeye, Infinia Hawkeye 4, and Discovery 670 (General Electric Medical Systems, Milwaukee, WI, USA), all with a crystal thickness of 5/8″ and equipped with a medium-energy parallel-hole collimator. For ^{177}Lu-DOTATATE examinations, we used a 20% energy window over the 208 keV photon peak, and for ^{111}In-octreotide examinations, a 20% energy window over the 245 keV photon peak was used. The clinical SPECT images were acquired 1–3 days post injection with 110–220 MBq ^{111}In-octreotide or 3–7.4 GBq ^{177}Lu-DOTATATE, with a 30-s frame time duration for 120 projections. The matrix size was 128×128 with a pixel size of 4.42 mm and a slice thickness of 4.42 mm. The CT images used in the SPECT/CT reconstructions, described below, were acquired using a 140-kV tube voltage, 2.5 mAs, and a rotation speed of 2.6 rpm. The matrix size was 512×512 with a pixel size of 0.98 mm and a slice thickness of 5 mm.

The Convolutional Neural Network

We constructed a deep convolutional U-net–shaped neural network for generation of synthetic intermediated projections (CUSIP) from a sparse set of projections, either 30 or 60 projections (*25*). Below we describe the method for 30 projections; the methodology is similar for 60 projections. The data for 60 projections was only evaluated with the phantom measurements, while the 30 projections was evaluated more extensively, as described below.

The CUSIP had a 3D U-net structure and was implemented in Microsoft's Cognitive Toolkit 2.6. The U-net structure consisted of encoder and decoder units with skip connections between the corresponding layers (Fig. 1). The input image consisted of 30 projections (projections 1, 5, 9…, 117) with a matrix size of 128×128, that was concatenated to generate a cubic matrix of (128×128×128). In this preprocessing step the voxel values were normalized to be within the range 0 to 2. The input image was convolved and down-sampled in the encoder part, which consisted of a series of convolutional layers with 3×3×3 kernels followed by a rectified linear unit (ReLU) activation function. Down-sampling was performed with max pooling layers with stride 2. After each down-sampling step, the feature channels were doubled.

As with the encoder, the decoder consisted of a series of convolution layers followed by a ReLU activation function. For up-sampling, the decoder unit used transposed convolutional layers with stride 1 followed by a ReLU activation function. The number of feature channels was halved after each up-sampling step.

Three different CUSIPs were trained to yield the following three SIP sets: a) projections 2, 6, 10…118; b) projections 3, 7, 11…119; and c) projections 4, 8, 12…120. These projection sets were cropped from the 128×128×128 matrix output images.

Training and Optimization

The three CUSIPs were trained by minimizing the mean square error loss function (L2-loss) between the difference in the network-generated SIP and the input projections. The Adam optimizer with a momentum of 0.05 and a linearly decreasing learning rate from 0.000012 to 0.000008 was used to minimize the loss function. Each CUSIP was trained using 352 input images (352×30 projections) and validated using 37 input images (37×30 projections). The training used

^{177}Lu and ^{111}In images, while validation only used ^{177}Lu images. The network was trained for 200 epochs with a mini-batch of one input image. To evaluate the network, we used a test set of SPECT/CT raw data from 15 patients treated with ^{177}Lu-DOTATATE together with SPECT/CT raw data from a phantom study (see below).

SPECT reconstructions

SPECT images for quality evaluation were reconstructed for three sets of projections: a) the 120 acquired projections (120), b) 30 projections using every fourth projection of the 120 (30), and c) 120 projections derived from 90 (3×30) SIPs generated from the 30 projections using the three CUSIPs (30-120IP). The SPECT/CT reconstructions were performed using two OSEM reconstruction algorithms with 6 subsets and 10 iterations.

The first was an AC-OSEM with Gaussian postfiltering (SD of 4 mm). In the second algorithm, the Sahlgrenska Academy Reconstruction code (SAREC) was used for attenuation, scatter, and ASCC-OSEM reconstruction (*9*). SAREC relies on MC simulations. The forward projections included simulation of photon attenuation, scattering, and collimator resolution with septal penetration. The scattering in the collimator is approximated with an experimentally determined photon-scattering kernel. The back projections include collimator resolution with septal penetration. In contrast to the AC-OSEM, no postfiltering was applied because the back-projector reduces noise.

Phantom Measurements

The Jaszczak SPECT Phantom with sphere inserts, with a 25:1 sphere-to-background activity concentration ratio, was used for image quality assessment. The phantom and the performed measurements are further described in the supplemental file.

Quantitative Image Quality Evaluation of Patient Images

We used the peak SNR (PSNR; Eq 1, Supplemental data), root mean square error (RMSE; Eq. 2, Supplemental data), and structural similarity (SSIM) index metrics (Eq 3, Supplemental data) to evaluate the image quality of the SIPs and the reconstructed SPECT images for the test set of 15 patients (*26*). These measures give an estimate of image quality compared to a reference image, in this case a reconstruction of all acquired 120 projections. We also performed this analysis on ASCC-OSEM 30 images that was postfiltered with a Gaussian filter, SD of 4 mm, (ASCC-OSEM 30GF).

Visual Evaluation of Image Quality

An experienced nuclear medicine physician (16 working years) visually evaluated the reconstructed SPECT/CT images of the test set, consisting of ^{177}Lu-DOTATATE SPECT images from 15 patients. The physician scored the image quality for each patient examination by ranking the six reconstructed images, i.e., AC-OSEM 30, AC-OSEM 30-120SIP, AC-OSEM 120, ASCC-OSEM 30, ASCC-OSEM 30-120SIP, and ASCC-OSEM 120. Categorial values from 1 to 6 were used as score values. The lowest score of 1 was given to the image with the poorest quality and a score of 6 to the image with the highest quality. For each patient, each of the 6 scores had to be

assigned to one of the 6 reconstructions, i.e. no double entries were possible. In addition, the observer noted whether the noise level was acceptable.

Activity Concentration in the Kidneys

In the test set with 15 patients, the kidney activity concentrations were determined by applying a VOI over the right and left kidneys in the reconstructed SPECT images. The VOIs were manually segmented in the CT images. The VOIs position in the SPECT image were manually adjusted for minimizing the effect of misposition caused by organ/patient movements between CT and SPECT acquisitions. The same VOI was used for all reconstructions of the same kidney and patient. Activity concentrations determined by using 30 or 30-120SIP projections were compared to activity concentrations determined by using the original 120 projections.

Statistics

For the quantitative evaluation of SPECT image quality, we analyzed the data using the paired Student's t-test. The scoring of the visual image quality was evaluated with the nonparametric Friedman's test, corrected for multiple testing by Tukey's honestly significant difference procedure. The difference between methods was evaluated using the paired Student's t-test for the AC-OSEM and ASCC-OSEM methods, respectively. The statistical tests were performed in MATLAB (MathWorks, Torrance, California, USA). A p-value less than 0.05 was considered to indicate statistical significance.

RESULTS

Each of the three CUSIPs was trained to 200 epochs for which loss of convergence was obtained, i.e. the validation loss function had reached its minimum. Visual inspection of the synthetic projections revealed a slightly smoother appearance compared to acquired projections (Fig. 2). The mean pixel difference between the acquired and synthetic projections was close to zero (-0.046), and both negative and positive differences were observed. The mean RMSE was 2.95 (Table 1). The PSNR was equal to 39.3 dB, and the SSIM was 0.926, indicating high structural similarity between the acquired projections and the SIPs; the SSIM for the aquired projections between the 15 patients was 0.846 (0.014).

The reconstructed SPECT images of the Jaszczak phantom demonstrated decreased noise with the 30-120SIP projection set compared to the 30 projection set (Fig. 3). For the AC-OSEM reconstructions, the SNR was clearly improved for the 30-120SIP compared to the 30 and 120 projection sets (Fig. 4). The image quality was higher for ASCC-OSEM reconstructions compared to AC-OSEM reconstruction (Figs. 3 and 4). For all projection sets, the recovery and SNR for ASCC-OSEM reconstruction were higher than AC-OSEM reconstruction. For ASCC-OSEM, the SNR was twofold higher for 120 compared to 30 projections. By CUSIP interpolation from the 30 projections to the 30-120SIP set, the SNR was in parity with ASCC-OSEM 120. In figure 4 we added data for 60 projections and data from a CUSIP that generates 60-120SIP. In the figure it is indicated that increasing number of SIPs increase SNR and slightly decrease recovery.

Figure 5 demonstrates the obtained SPECT image quality with ASCC-OSEM using the 30, 30-120SIP, and 120 projection sets. A higher noise level was observed in the reconstruction

with 30 projections. With an increased number of projections, with either the 30-120SIP or the 120 projection set, the noise level was decreased, and a smoother activity distribution was observed. The image difference demonstrates a higher deviation in pixel values between the 30 and 120 projection sets as compared to the pixel values between the 30-120SIP and 120 projection sets. The RMSE, PSNR and SSIM was statistically significantly improved between the 30 and 30-120SIP sets, both for the AC-OSEM ($p<0.001$) and ASCC-OSEM ($p<0.001$) reconstructions (Table 2). In contrast, the RMSE and PSNR had a tendency to get worse for the postfiltered ASCC-OSEM, though not statistically significant. The SSIM was high (0.993 – 0.996) for all ASCC-OSEM reconstructions. The SSIM for the SPECT images between the 15 patients was 0.962 (0.0190). Different selection of the 30 projection in 30-120SIP revealed non-statistical different PSNR, RSME and SSIM (data not shown), indicating that the method is robust.

When ranked by an experienced nuclear medicine physician, the ASCC-OSEM drew the highest scores, in which all projection sets had higher scores than the highest score for the AC-OSEM reconstructions (Fig. 6). However, when using only 30 projections, the observer judged almost all SPECT images to have unacceptable noise levels, at 13/15 for AC-OSEM and 14/15 for ASCC-OSEM. By using 30-120SIP or 120 projections, almost all reconstructed SPECT images had acceptable noise levels; at 1/15 for AC-OSEM 120 and 1/15 for ASCC-OSEM 30-120SIP had an unacceptable level.

For ASCC-OSEM, the increased scores for the 30-120SIP and 120 projections were statistically significant. The reconstruction with 30-120SIP (mean score=5.2) was in parity with 120 projections (mean score=5.8), with no statistically significant difference.

The determination of the kidney activity concentration showed small variations among the different reconstruction methods (Fig. 7). The ASCC-OSEM 30-120SIP underestimated the activity concentration slightly (3% for left kidney and 2.5% for right kidney) compared to the ASCC-OSEM 120. No other statistical differences were observed.

DISCUSSION

The use of artificial intelligence and especially the field of deep learning are expanding. For gamma camera imaging, the number of publications is still limited, while positron emission tomography (PET) findings are more widely described. One of the most frequently reported topics is the generation of synthetic attenuation maps for attenuation corrections of PET images (*27*). We adopted a similar convolutional neural network as in these studies, i.e., a U-net structure where the input images of the sparse intermediate projections are down-sampled and up-sampled for obtaining the SIP. The generated SIPs had a reduced noise level compared to the original data and a high structural similarity with the original projections, as measured by SSIM. Inserting these SIPs into the reconstruction revealed improved image quality compared to reconstructions of the sparse projection datasets, and the noise level especially was substantially reduced. As a comparison, we also applied filtering of the SPECT images generated with 30 projections, which resulted in smoother images but no gain in RMSE or PSNR, as also was the case with the addition of SIPs. The advantage with SIPs, in comparison with postfiltering, is that counts are added into the reconstruction. Thereby, the use of SIPs might be an alternative way of filtering SPECT images, which have to be studied further.

We added ^{111}In-octreotide SPECT images for increasing the training set by 25%. Similar cameras and collimators were used in these investigations. The slightly higher emitted photon energy from ^{111}In (245 vs. 208 keV) causes a slightly poorer resolution and might therefore have contributed to reduced recovery for OSEM reconstruction with SIPs compared to the full set of projections. However, the addition of ^{111}In images reduced the loss in both training and validation, indication a beneficial value of increasing the training set with ^{111}In images. This subject will be further explored in upcoming studies which also will be focused on improving ^{111}In imaging with CUSIP.

The gamma cameras had a crystal thickness of 5/8" and used body contour orbits. These camera specific parameters might also influence the CUSIPs performance when applied on projections from other cameras. In this study we don't have data for such extended analysis. As with all AI-development the limited amount of data is problematic. Nevertheless, with research sites having others cameras we intend to study this issue further.

In this study, we used two reconstruction protocols: a low-resolution OSEM protocol with AC-OSEM and a high-resolution OSEM protocol with ASCC-OSEM. With the use of AC-OSEM for ^{177}Lu-DOTATATE, a dose-response relationship for pancreatic tumors has been described, as well as dosimetry for various organs, e.g., the kidneys (*13,14,28*). Our results demonstrate that it should be feasible to reduce the number of projections and add SIPs and obtain SPECT image quality similar to that with the full set of projections. There was a slight decrease in recovery in the phantom measurements, which could explain the slightly decreased kidney activity concentration estimate. This decrease is probably the result of the inherent poor resolution in AC-OSEM reconstruction rather than of the minor resolution loss when applying 30-120SIP. When we applied the high-resolution method, ASCC-OSEM, we saw a similar increase in image quality, but with a more pronounced loss in recovery. The kidney activity concentration decreased by about 2% compared to the full set of projections. Despite the higher resolution of ASCC-OSEM, however, the typical resolution recovery for a kidney is about 85%, indicating that a similar degree of adjustment needs to be performed in OSEM reconstruction with a 120 or 30-120SIP projection set (*29*).

For both reconstruction methods, the variation in kidney activity concentration estimates decreased for OSEM 30-120SIPs compared to the 30 projection set. The observer also noted that reconstruction with 30 projections was too noisy for clinical interpretation. With a high noise level

in the image, reporting response or regrowth of small disseminate tumors would be challenging. Nevertheless, the overall score for ASCC-OSEM 30 was higher than the AC-OSEM 30-120SIP and AC-OSEM 120 reconstructions, which were judged to have acceptable noise levels. This contradiction is probably due to the used scoring system that forced the observer to use all scores for a patient. This might result in an inaccuracy of incorporating the negatively influences of high noise level in the overall score, and thereby indicating a better image quality for ASCC-OSEM 30 than AC-OSEM 120.

For the ASCC-OSEM, we used MC-based reconstruction. The benefit with this approach is that attenuation, scatter, and collimator-detector response are corrected simultaneously in the forward projection, which seems to generate images that might be slightly improved or in parity with the compensation methods applied by different vendors (*9-11*). Despite the possible improvements that can be obtained with MC-based reconstruction, results similar to those presented here for 30-120SIP will most probably hold true for all other OSEM methodologies with robust attenuation, scatter, and collimator-detector response correction.

CONCLUSION

In the present study, we demonstrated that SPECT image quality, as measured by RMSE, PSNR, SNR, and SSIM, can be improved by adding SIPs to sparsely sampled projections. The visual inspection revealed that SPECT images generated with sparsely collected projections had unacceptable image quality, whereas the SPECT/CT reconstruction with the 30-120SIP set had an image quality similar to that of the full set of projections. This similarity enables the use of synthetic projections for acquisition time reduction in clinical protocols, which is beneficial for patient comfort and minimizes the risk of patient movement under image acquisition. Additionally, it enhances the possibility of adding acquisition time points or increasing the number of bed positions

with each time point in full clinical schedules, which can be important for improved accuracy of the pharmacokinetics in the dosimetry protocol.

DISCLOSURE

No potential conflicts of interest relevant to this article exist.

ACKNOWLEDGMENTS

This work was supported by the Swedish Cancer Society, Swedish Radiation Safety Authority, King Gustav V Jubilee Clinic Cancer Research Foundation, Swedish Research Council, and Swedish State under the agreement between the Swedish government and the county councils, the ALF agreement.

KEY POINTS

Question: Can SPECT acquisition be decreased without image degradation by adding deep learning–generated synthetic intermediate projections?

Pertinent Findings: The results of this cohort study of 15 patients treated with ^{177}Lu-DOTATATE show that the SPECT acquisition time can be reduced by a factor of 4 while still yielding image quality similar to that for a full set of 120 projections.

Implications for Patient Care: Reducing SPECT acquisition time will improve patient comfort during investigation, reduce risk for image artefacts from patient movement, and offer the opportunity to increase the number of measurement time points after injection of ^{177}Lu-radiopharmaceuticals for improved pharmacokinetic description and patient dosimetry.

REFERENCES

1. Strosberg J, El-Haddad G, Wolin E, et al. Phase 3 Trial of 177Lu-Dotatate for Midgut Neuroendocrine Tumors. *N Engl J Med.* 2017;376:125-135.

2. von Eyben FE, Roviello G, Kiljunen T, et al. Third-line treatment and (177)Lu-PSMA radioligand therapy of metastatic castration-resistant prostate cancer: a systematic review. *Eur J Nucl Med Mol Imaging.* 2018;45:496-508.

3. Garske-Roman U, Sandstrom M, Fross Baron K, et al. Prospective observational study of (177)Lu-DOTA-octreotate therapy in 200 patients with advanced metastasized neuroendocrine tumours (NETs): feasibility and impact of a dosimetry-guided study protocol on outcome and toxicity. *Eur J Nucl Med Mol Imaging.* 2018;45:970-988.

4. Cremonesi M, Ferrari ME, Bodei L, et al. Correlation of dose with toxicity and tumour response to (90)Y- and (177)Lu-PRRT provides the basis for optimization through individualized treatment planning. *Eur J Nucl Med Mol Imaging.* 2018;45:2426-2441.

5. Hagmarker L, Svensson J, Ryden T, et al. Bone Marrow Absorbed Doses and Correlations with Hematologic Response During (177)Lu-DOTATATE Treatments Are Influenced by Image-Based Dosimetry Method and Presence of Skeletal Metastases. *J Nucl Med.* 2019;60:1406-1413.

6. He B, Du Y, Segars WP, et al. Evaluation of quantitative imaging methods for organ activity and residence time estimation using a population of phantoms having realistic variations in anatomy and uptake. *Med Phys.* 2009;36:612-619.

7. Hudson HM, Larkin RS. Accelerated image reconstruction using ordered subsets of projection data. *IEEE Trans Med Imaging.* 1994;13:601-609.

8. Tran-Gia J, Lassmann M. Characterization of Noise and Resolution for Quantitative (177)Lu SPECT/CT with xSPECT Quant. *J Nucl Med.* 2019;60:50-59.

9. Ryden T, Heydorn Lagerlof J, Hemmingsson J, et al. Fast GPU-based Monte Carlo code for SPECT/CT reconstructions generates improved (177)Lu images. *EJNMMI Phys.* 2018;5:1.

10. Gustafsson J, Brolin G, Ljungberg M. Monte Carlo-based SPECT reconstruction within the SIMIND framework. *Phys Med Biol.* 2018;63:245012.

11. Elschot M, Lam MG, van den Bosch MA, Viergever MA, de Jong HW. Quantitative Monte Carlo-based 90Y SPECT reconstruction. *J Nucl Med.* 2013;54:1557-1563.

12. Ljungberg M, Celler A, Konijnenberg MW, et al. MIRD Pamphlet No. 26: Joint EANM/MIRD Guidelines for Quantitative 177Lu SPECT Applied for Dosimetry of Radiopharmaceutical Therapy. *J Nucl Med.* 2016;57:151-162.

13. Sandstrom M, Garske U, Granberg D, Sundin A, Lundqvist H. Individualized dosimetry in patients undergoing therapy with (177)Lu-DOTA-D-Phe (1)-Tyr (3)-octreotate. *Eur J Nucl Med Mol Imaging.* 2010;37:212-225.

14. Sandstrom M, Garske-Roman U, Granberg D, et al. Individualized dosimetry of kidney and bone marrow in patients undergoing 177Lu-DOTA-octreotate treatment. *J Nucl Med.* 2013;54:33-41.

15. Santoro L, Mora-Ramirez E, Trauchessec D, et al. Implementation of patient dosimetry in the clinical practice after targeted radiotherapy using [(177)Lu-[DOTA0, Tyr3]-octreotate. *EJNMMI Res.* 2018;8:103.

16. Garkavij M, Nickel M, Sjogreen-Gleisner K, et al. 177Lu-[DOTA0,Tyr3] octreotate therapy in patients with disseminated neuroendocrine tumors: Analysis of dosimetry with impact on future therapeutic strategy. *Cancer.* 2010;116:1084-1092.

17. Marin G, Vanderlinden B, Karfis I, et al. A dosimetry procedure for organs-at-risk in (177)Lu peptide receptor radionuclide therapy of patients with neuroendocrine tumours. *Phys Med.* 2018;56:41-49.

18. Delker A, Fendler WP, Kratochwil C, et al. Dosimetry for (177)Lu-DKFZ-PSMA-617: a new radiopharmaceutical for the treatment of metastatic prostate cancer. *Eur J Nucl Med Mol Imaging.* 2016;43:42-51.

19. Hou X, Zhao W, Beauregard JM, Celler A. Personalized kidney dosimetry in (177)Lu-octreotate treatment of neuroendocrine tumours: a comparison of kidney dosimetry estimates based on a whole organ and small volume segmentations. *Phys Med Biol.* 2019;64:175004.

20. Chicheportiche A, Grozinsky-Glasberg S, Gross DJ, et al. Predictive power of the post-treatment scans after the initial or first two courses of [(177)Lu]-DOTA-TATE. *EJNMMI Phys.* 2018;5:36.

21. Violet J, Jackson P, Ferdinandus J, et al. Dosimetry of (177)Lu-PSMA-617 in Metastatic Castration-Resistant Prostate Cancer: Correlations Between Pretherapeutic Imaging and Whole-Body Tumor Dosimetry with Treatment Outcomes. *J Nucl Med.* 2019;60:517-523.

22. Hippelainen E, Tenhunen M, Maenpaa H, Sohlberg A. Quantitative accuracy of (177)Lu SPECT reconstruction using different compensation methods: phantom and patient studies. *EJNMMI Res.* 2016;6:16.

23. Beauregard JM, Hofman MS, Pereira JM, Eu P, Hicks RJ. Quantitative (177)Lu SPECT (QSPECT) imaging using a commercially available SPECT/CT system. *Cancer Imaging.* 2011;11:56-66.

24. Kabasakal L, Toklu T, Yeyin N, et al. Lu-177-PSMA-617 Prostate-Specific Membrane Antigen Inhibitor Therapy in Patients with Castration-Resistant Prostate Cancer: Stability, Bio-distribution and Dosimetry. *Mol Imaging Radionucl Ther.* 2017;26:62-68.

25. Ronneberger O. FP, Brox T. U-Net: Convolutional Networks for Biomedical Image Segmentation May 18, 2015; https://arxiv.org/abs/1505.04597. Accessed November 08, 2018.

26. Wang Z, Bovik AC, Sheikh HR, Simoncelli EP. Image quality assessment: from error visibility to structural similarity. *IEEE Trans Image Process.* 2004;13:600-612.

27. Spuhler KD, Gardus J, 3rd, Gao Y, DeLorenzo C, Parsey R, Huang C. Synthesis of Patient-Specific Transmission Data for PET Attenuation Correction for PET/MRI Neuroimaging Using a Convolutional Neural Network. *J Nucl Med.* 2019;60:555-560.

28. Sandstrom M, Garske-Roman U, Johansson S, Granberg D, Sundin A, Freedman N. Kidney dosimetry during (177)Lu-DOTATATE therapy in patients with neuroendocrine tumors: aspects on calculation and tolerance. *Acta Oncol.* 2018;57:516-521.

29. Sundlov A, Sjogreen-Gleisner K, Svensson J, et al. Individualised (177)Lu-DOTATATE treatment of neuroendocrine tumours based on kidney dosimetry. *Eur J Nucl Med Mol Imaging.* 2017;44:1480-1489.

Table 1. Clinical SPECT acquiring protocols for ^{177}Lu dosimetry.

Study	Treatment	Acquisition time (min)	Number of projections	Frame time (s)	Bed	Measuring times (h.p.i.)
Marin et al. (*17*)	^{177}Lu-DOTATATE	21.3–42.7	64	40–80	1	4, 24, 144–192
Sandström et al. (*13*)	^{177}Lu-DOTATATE	30	60	60	1	1, 24, 96, 168
Sandström et al. (*14*)	^{177}Lu-DOTATATE	30	120	30	1	1, 24, 96, 168
Hagmarker et al. (*5*)	^{177}Lu-DOTATATE	30	120	30	1	24
Santoro et al. (*15*)	^{177}Lu-DOTATATE	22.5	60	45	1	4, 24, 72, 192
Garkavij et al. (*16*)	^{177}Lu-DOTATATE	22.5	60	45	1	24/96
Delker at al. (*18*)	^{177}Lu-PSMA-617	21.3	128	20	1	24, 48, 72
Kabasakal et al. (*24*)	^{177}Lu-PSMA	20/bed	96	25	2	24
Hou et al. (*19*)	^{177}Lu-DOTATATE	12–16	96	15–20	1	4, 24, 72
Chichepotiche et al. (*20*)	^{177}Lu-DOTATATE	15	60	30	1	20, 25, 168
Beauregard et al. (*23*)	^{177}Lu-DOTATATE	8–12	96	10–15	1	4, 24, 96
Violet et al. (*21*)	^{177}Lu-PSMA-617	(8–12)/bed	96	10–15	2-3	4, 24, 96
Hippeläinen et al. (*22*)	^{177}Lu-DOTATATE	10.7	64	20	1	24, 48, 168

Table 2. The image quality metrics RMSE, PSNR, and SSIM for the synthetic intermediate projections (SIPs) and SPECT images in the test group of patients.

Images	**RMSE**	**PSNR**	**SSIM**
SIPs	2.95 (0.77)	39.2 (3.8)	0.926 (0.061)
AC-OSEM 30	0.147 (0.060)	47.2 (3.5)	0.989 (0.008)
AC-OSEM 30-120SIP	0.109 (0.044)***	49.5 (3.3)***	0.993 (0.005)***
ASCC-OSEM 30	0.259 (0.101)	49.0 (3.5)	0.993 (0.005)
ASCC-OSEM 30GF	0.273 (0.162)	48.3 (2.5)	0.995 (0.004)**
ASCC-OSEM 30-120SIP	0.195 (0.091)***	50.8 (3.2)***	0.996 (0.003)***

** P<0.01, *** P<0.001

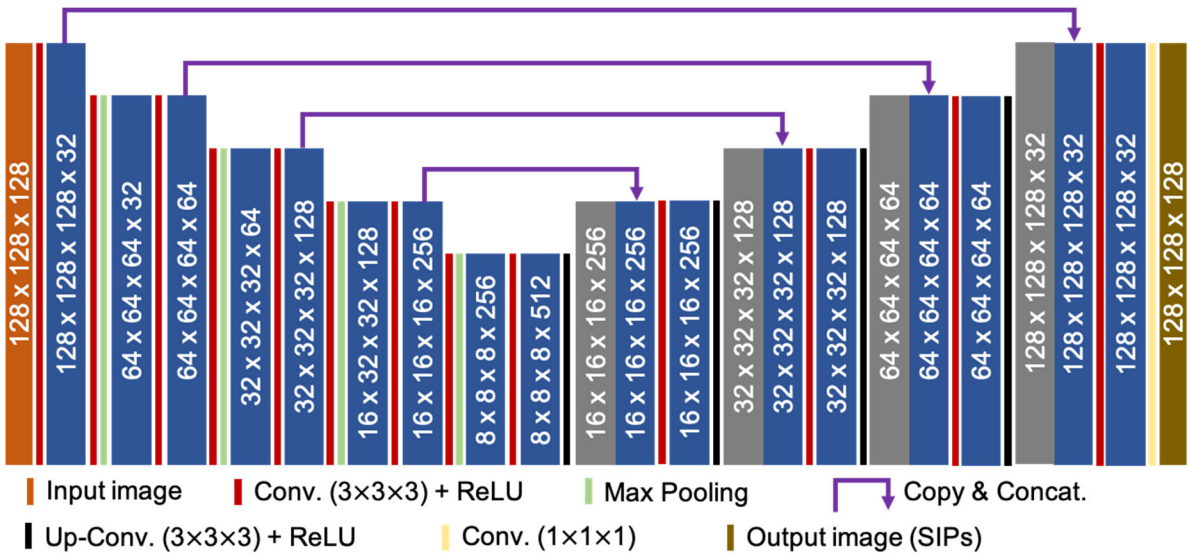

Figure 1. Schematic illustration of CUSIP; the convolutional U-net–shaped neural network for generation of synthetic intermediate projections. Numbers indicate image size and number of features at each layer.

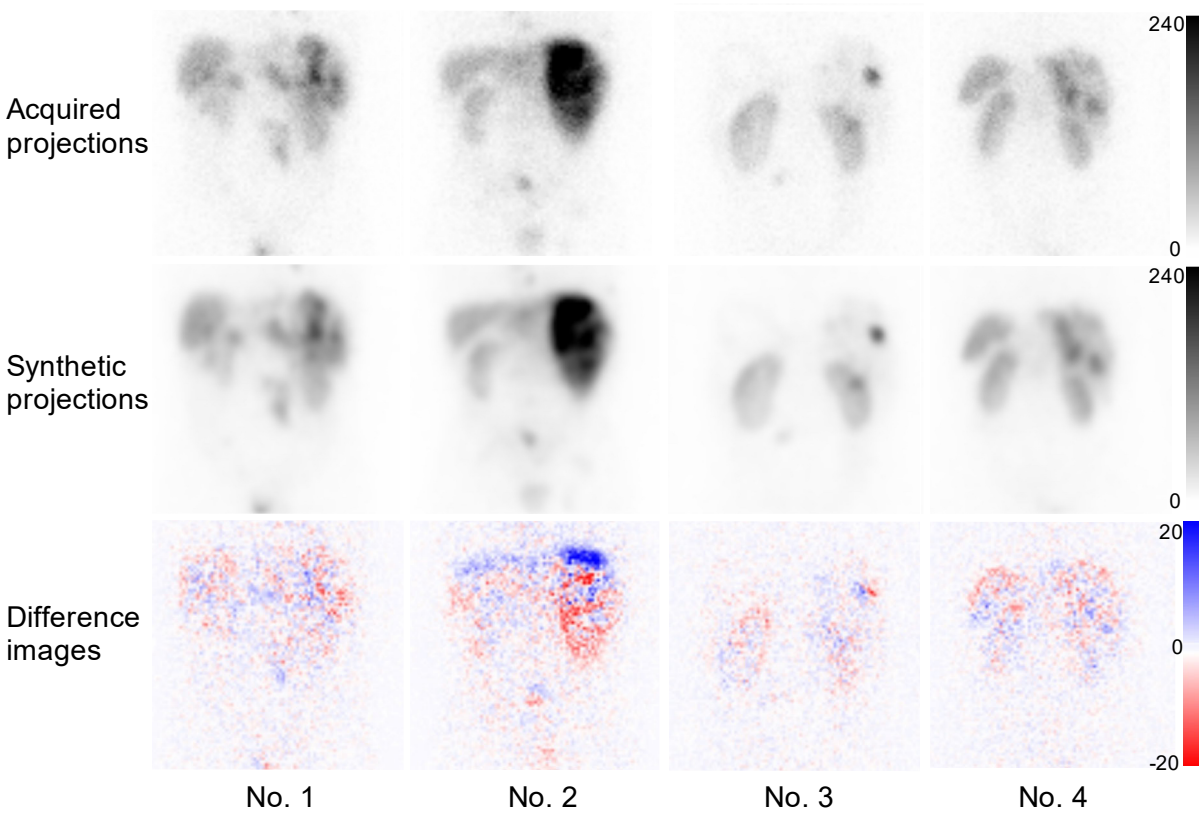

Figure 2. Comparison of acquired projection with the corresponding synthetic intermediate projection in four of the patients in the test group (Nos. 1–4). The difference images display the pixel value dissimilarities between the acquired and synthetic projections. Blue indicates positive pixel values, white indicates no differences, and red indicates negative values. Unit of colorbar is counts.

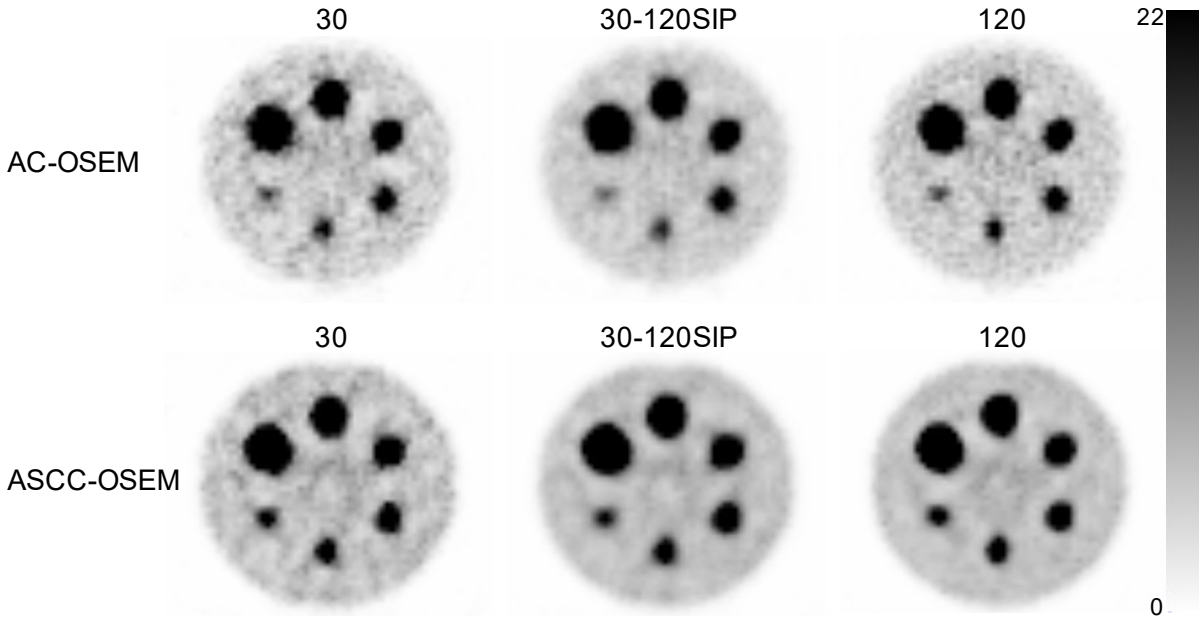

Figure 3. SPECT/CT reconstructions of the Jaszczak phantom with six hot spheres having 25 times higher ^{177}Lu activity concentration compared to background. The AC-OSEM and ASCC-OSEM reconstructed with 30, 30-120SIP, and 120 projections. Unit of color bar is arbitrary voxel values.

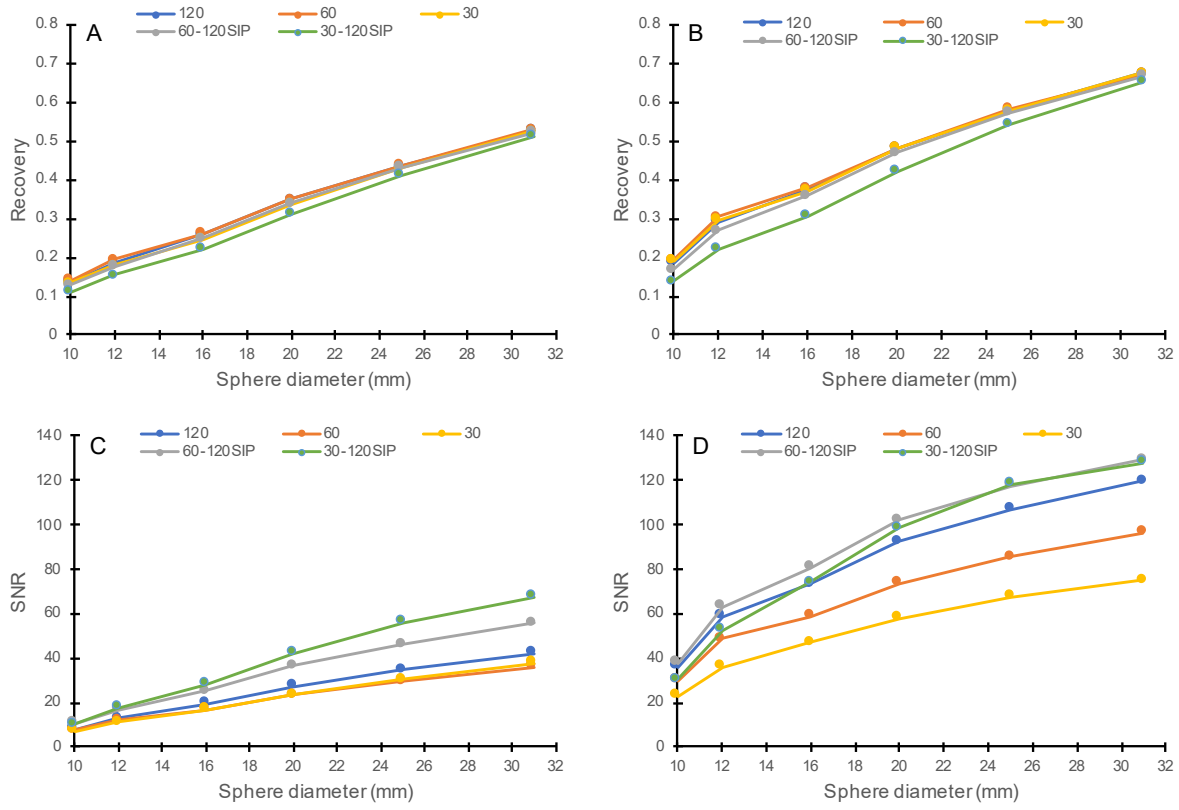

Figure 4. The recovery and signal-to-noise ratio (SNR) for ^{177}Lu determined in the various hot spheres in the Jaszczak phantom for (A, C) the AC-OSEM SPECT/CT reconstruction and (B, D) the ASCC-OSEM SPECT/CT reconstruction with 30 (yellow line), 60 (orange line), 120 (blue line), 60-120SIP (gray line), and 30-120SIP (green line) projections.

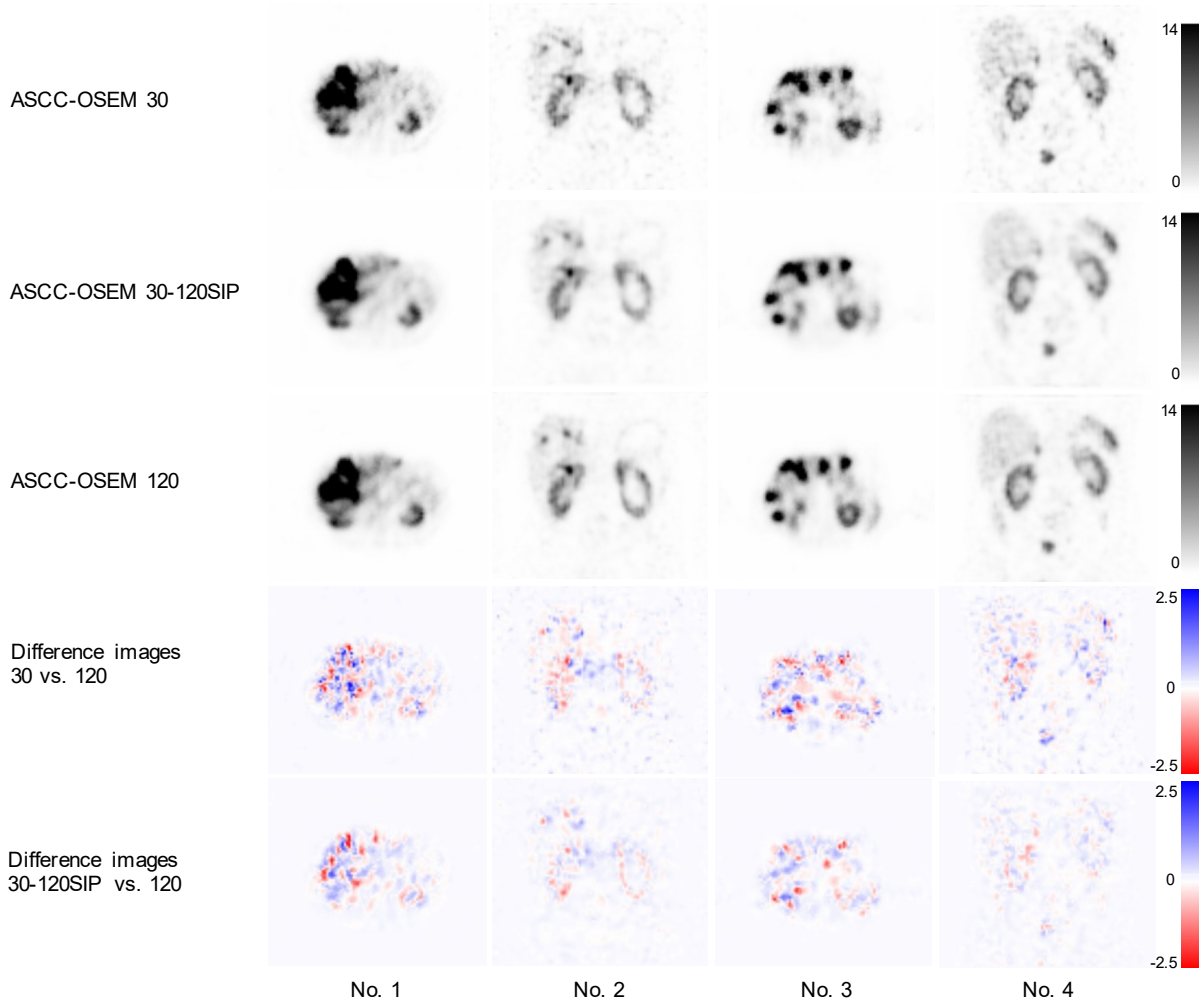

Figure 5. Comparison of ASCC-OSEM reconstruction with 30, 30-120SIP, and 120 projections in four (Nos. 1–4) of the 15 patients in the test set. The difference images display the pixel value dissimilarities between the ASCC-OSEM 30 versus ASCC-OSEM 120 and ASCC-OSEM 30-120SIP versus ASCC-OSEM 120. The blue indicates positive pixel values, white indicates no differences, and red indicates negative values. Unit of colorbar is arbitrary voxel values.

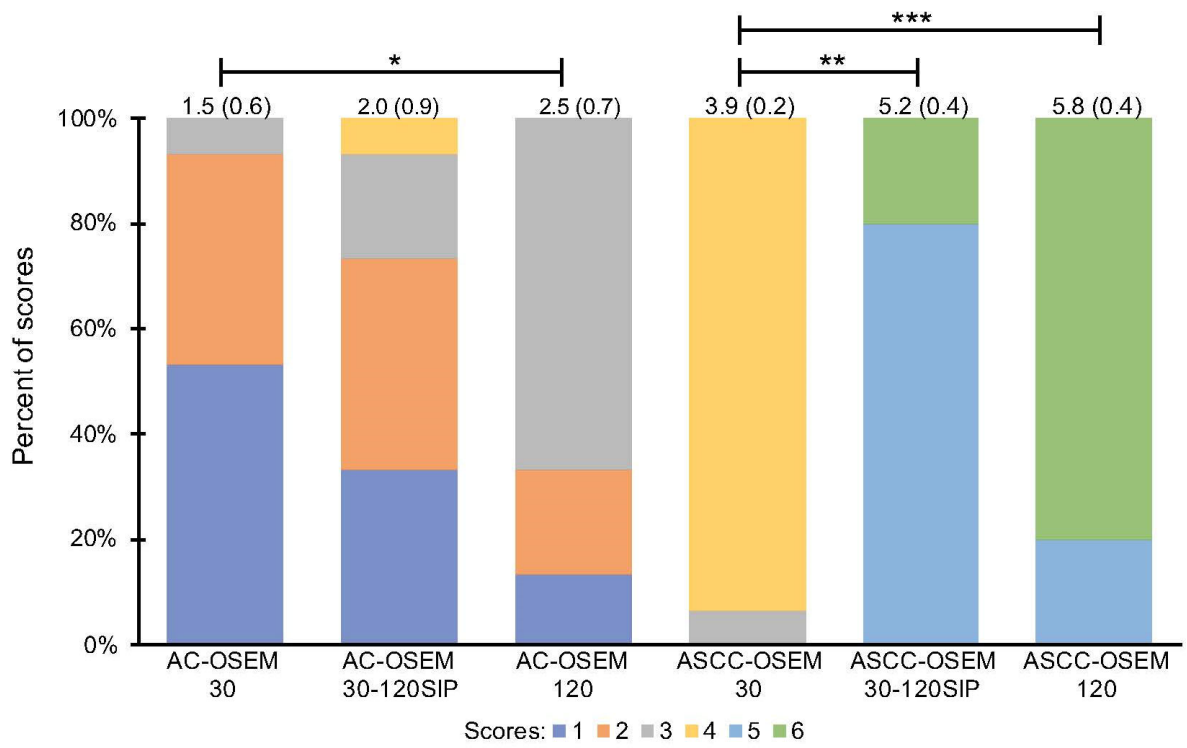

Figure 6. The evaluation scores for the SPECT/CT reconstructions with AC-OSEM and ASCC-OSEM. Mean scores and standard deviations shown at the top of the bars. The stars indicate statistical significance of the scores between the projection sets within the AC-OSEM and ASCC-OSEM reconstructions, respectively; * $0.01 \leq p < 0.05$, ** $0.001 \leq p < 0.01$, *** $p < 0.001$.

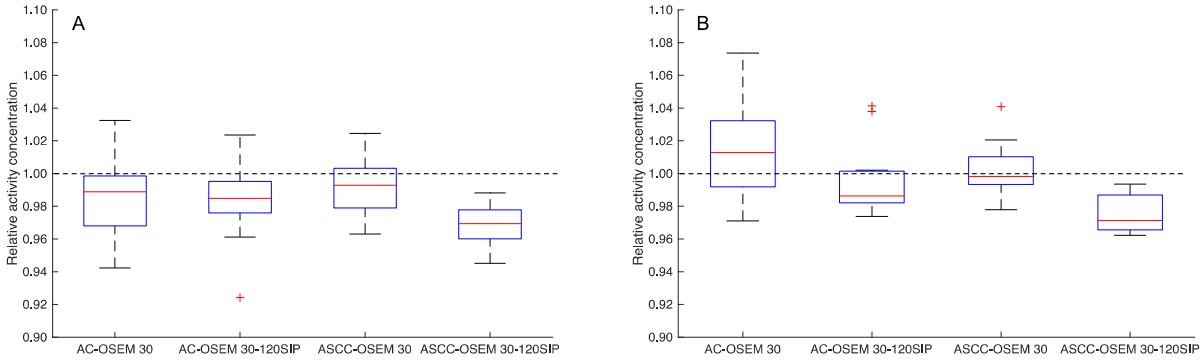

Figure 7. The relative kidney activity concentration for the AC-OSEM and ASCC-OSEM reconstructions with 30 and 30-120SIP projections vs. the reconstruction with 120 projections. The relative activity concentration was determined in the left (A) and right kidneys (B).

Supplemental data-set for:

Deep learning generation of synthetic intermediate projections improves ^{177}Lu SPECT images reconstructed with sparsely acquired projections

Phantom measurements

The Jaszczak SPECT Phantom was used for image quality assessment. The phantom is cylindrical and includes six hollow spheres, with inner diameters of 10, 12, 16, 20, 25, and 31 mm, respectively. The phantom and the spheres were filled with an aqueous solution containing ^{177}Lu-DOTATATE. The ratio between the activity concentration in the spheres and the background compartment of the phantom was approximately 25. In the reconstructed images, the signal-to-noise ratios (SNRs) were calculated as follows:

$$SNR = \frac{N_S - N_B}{\sigma_B} \quad (1)$$

where N_S is the mean counts in a volume of interest (VOI_S) equal to the inner diameter of the sphere of interest. N_B and σ_B is the mean and standard deviation of the counts in 20 VOIS, equal the size of VOI_S; placed far away from the hot spheres in the Jaszczak phantom. The recovery coefficient was calculated as the measured activity within the sphere in the SPECT image compared to true activity.

Quantitative image quality evaluation of patient images

The image quality of the synthetic intermediate projections (SIPs) and the reconstructed SPECT images for the test set of 15 patients were evaluated by the peak signal-to-noise ratio (PSNR; Eq 1), root mean square error (RMSE; Eq. 2) and structural similarity index metrics (SSIM; Eq 3).

These measures are estimate of image quality compared to the reference image. For the SIPs the reference images are the acquired projections. The reference SPECT image is the reconstruction of all 120 acquired projections.

The PSNR is derived from the mean square error and specifies the ratio of the maximal pixel intensity to the power of distortion compare the refence image (RI):

$$\text{PSNR} = 20\, log_{10}\left(\frac{MAX}{RMSE}\right) \quad (1)$$

where MAX is maximum voxel value in the image.

RMSE is square root of the quadratic mean of differences between image (IM) and RI:

$$\text{RMSE} = \sqrt{\frac{1}{\text{nml}}\sum_x^n \sum_y^m \sum_z^l (IM(x,y,z) - RI(x,y,z))^2} \quad (2)$$

n, m and l are the number of voxels in each direction of the SPECT image. $IM(x,y,z)$ and $RI(x,y,z)$ refer to the x, y and z coordinates in the SPECT images. For projection images IM and RI are changed to represent 2D images; $IM(x,y)$ and $RI(x,y)$.

SSIM is a perception-based measure that considers image degradation as perceived change in structural information (I). The values of SSIM range from 0 to 1 where a higher value indicates higher similarity between the images. SSIM where calculated by 3×3×3 kernel size as follows:

$$\text{SSIM (IM, RI)} = \frac{(2\mu_{IM}\mu_{RI}+c_1)(2\sigma_{IMRI}+c_2)}{(\mu_{IM}^2+\mu_{RI}^2+c_1)(\sigma_{IM}^2+\sigma_{RI}^2+c_2)} \quad (3)$$

where μ_{IM} is the average of IM, μ_{RI} is the average of RI, σ_{IM}^2 is variance of IM, σ_{RI}^2 is the variance of RI, σ_{IMRI} is covariance of IM and RI. Two variables c_1 and c_2 are used to stabilize the division with a weak denominator defined as:

$c_1 = (K_1 L)^2$, $c_2 = (K_2 L)^2$

where L is the dynamic range of the voxel-values, K_1 and K_2 set by default to 0.01 and 0.03 respectively.

Reference

1. Wang Z, Bovik AC, Sheikh HR, Simoncelli EP. Image quality assessment: from error visibility to structural similarity. *IEEE Trans Image Process.* 2004;13:600-612.